

RESEARCH ARTICLE

Inclusion of maintenance energy improves the intracellular flux predictions of CHO

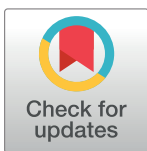
Diana Széliová^{1,2☯}, Jerneja Štor^{1,3☯}, Isabella Thiel³, Marcus Weinguny^{1,3}, Michael Hanscho¹, Gabriele Lhota³, Nicole Borth^{1,3}, Jürgen Zanghellini^{1,2☯*}, David E. Ruckerbauer^{1,2,3☯*}, Isabel Rocha^{4,5}

1 acib – Austrian Centre of Industrial Biotechnology, Vienna, Austria, **2** Department of Analytical Chemistry, University of Vienna, Vienna, Austria, **3** Department of Biotechnology, University of Natural Resources and Life Sciences, Vienna, Austria, **4** Centro de Engenharia Biológica, Universidade do Minho, Braga, Portugal, **5** ITQB-NOVA—Instituto de Tecnologia Química e Biológica António Xavier, Universidade Nova de Lisboa, Oeiras, Portugal

☯ These authors contributed equally to this work.

☯ Current address: Department of Analytical Chemistry, University of Vienna, Vienna, Austria

* juergen.zanghellini@univie.ac.at (JZ); ruckerbaud85@univie.ac.at (DER)



OPEN ACCESS

Citation: Széliová D, Štor J, Thiel I, Weinguny M, Hanscho M, Lhota G, et al. (2021) Inclusion of maintenance energy improves the intracellular flux predictions of CHO. *PLoS Comput Biol* 17(6): e1009022. <https://doi.org/10.1371/journal.pcbi.1009022>

Editor: Jason M. Haugh, North Carolina State University, UNITED STATES

Received: April 14, 2021

Accepted: April 28, 2021

Published: June 11, 2021

Peer Review History: PLOS recognizes the benefits of transparency in the peer review process; therefore, we enable the publication of all of the content of peer review and author responses alongside final, published articles. The editorial history of this article is available here: <https://doi.org/10.1371/journal.pcbi.1009022>

Copyright: © 2021 Széliová et al. This is an open access article distributed under the terms of the [Creative Commons Attribution License](https://creativecommons.org/licenses/by/4.0/), which permits unrestricted use, distribution, and reproduction in any medium, provided the original author and source are credited.

Data Availability Statement: All data and code are available at Mendeley Data <http://dx.doi.org/10.17632/p973bk79ck.1>.

Abstract

Chinese hamster ovary (CHO) cells are the leading platform for the production of biopharmaceuticals with human-like glycosylation. The standard practice for cell line generation relies on trial and error approaches such as adaptive evolution and high-throughput screening, which typically take several months. Metabolic modeling could aid in designing better producer cell lines and thus shorten development times. The genome-scale metabolic model (GSMM) of CHO can accurately predict growth rates. However, in order to predict rational engineering strategies it also needs to accurately predict intracellular fluxes. In this work we evaluated the agreement between the fluxes predicted by parsimonious flux balance analysis (pFBA) using the CHO GSMM and a wide range of ¹³C metabolic flux data from literature. While glycolytic fluxes were predicted relatively well, the fluxes of tricarboxylic acid (TCA) cycle were vastly underestimated due to too low energy demand. Inclusion of computationally estimated maintenance energy significantly improved the overall accuracy of intracellular flux predictions. Maintenance energy was therefore determined experimentally by running continuous cultures at different growth rates and evaluating their respective energy consumption. The experimentally and computationally determined maintenance energy were in good agreement. Additionally, we compared alternative objective functions (minimization of uptake rates of seven nonessential metabolites) to the biomass objective. While the predictions of the uptake rates were quite inaccurate for most objectives, the predictions of the intracellular fluxes were comparable to the biomass objective function.

Author summary

There is an increasing demand for protein pharmaceuticals, especially monoclonal antibodies. Chinese Hamster Ovary (CHO) are currently the leading production host due to

Funding: This work has been supported the COMET center acib: Next Generation Bioproduction, which is funded by BMK, BMDW, SFG, Standortagentur Tirol, Government of Lower Austria and Vienna Business Agency in the framework of COMET - Competence Centers for Excellent Technologies. The COMET-Funding Program is managed by the Austrian Research Promotion Agency FFG; D.S., J.S., M.W., M.H., D. E.R. This work has also been supported by the PhD program BioToP of the Austrian Science Fund (FWF Project W1224); D.S., M.W. The funders had no role in study design, data collection and analysis, decision to publish, or preparation of the manuscript.

Competing interests: The authors have declared that no competing interests exist.

their ability to perform human-like post-translational modifications. However, it typically takes several months of trial-and-error approaches to develop a high-producer cell line. Metabolic modelling has the potential to make cell line and process development faster and cheaper by predicting targeted modifications to the cell line genome, cultivation medium or bioprocess. In fact, genome-scale metabolic reconstructions of CHO are already available, and ready for use in cell line development. However, in order to successfully use these models, we need to make sure that they are able to accurately predict metabolic phenotypes. Here we use genome-scale metabolic models of CHO to evaluate the models' ability to correctly predict intracellular flux distributions. We find that a crucial key ingredient for the correct estimation of central carbon fluxes is the non-growth associated maintenance energy (mATP). We estimated mATP computationally and confirmed it experimentally. Adding this single constraint leads to significantly better predictions of intracellular fluxes, especially in glycolysis and the tricarboxylic acid cycle.

Introduction

Chinese hamster ovary (CHO) cells are currently the leading production host for the synthesis of complex biopharmaceuticals with human-like post-translational modifications [1]. Products made in CHO belong to the top-selling drugs on the market (e.g. Humira) [2]. The increasing demand for CHO-derived products requires advances in cell line and process development. Until now, significant improvements in productivity, product yield and growth rate of the cells have been achieved by media optimization and high-throughput screening for good producers [3, 4]. However, the development of high producer cell lines is laborious, expensive and takes several months for each new product [5]. Systems biology approaches such as metabolic modeling might push the productivity even further, shorten the development times for new products and improve the product quality by elucidating potential bottlenecks in metabolism and suggesting genetic engineering or feed/media optimization strategies [6, 7].

In 2016, a community-derived, consensus genome-scale metabolic model (GSMM) of CHO was published [8] and several updates have been made since [9–11]. These serve as a basis for applying genome-scale metabolic modeling to CHO. Simulations based on this model suggested huge potential for improved protein productivities [8]. Indeed, productivity was recently increased by implementing targeted knock-outs of several secreted host cell proteins. These results were consistent with the predictions of the CHO GSMM coupled with the secretory pathway model [11], which showed that these knock-outs would free up cellular resources [12].

To successfully use modeling for the rational design of new engineering strategies, accurate predictions of cellular phenotypes are essential. Previously we showed that a GSMM can accurately predict growth rates if supplied with accurate exchange rates of (essential) amino acids (AAs) and correctly determined biomass composition [13–15]. However, the model also needs to accurately predict intracellular fluxes. Previously it was shown that biomass composition [16] as well as extracellular exchange rates [17] have a big impact on the predicted intracellular fluxes. However, the validation of the flux predictions by the CHO GSMM with experimental data has been done only in one study so far [9].

In this work, we compare fluxes predicted by parsimonious flux balance analysis (pFBA), using the GSMM of CHO [8], against 20 ¹³C metabolic flux data sets across producer and non-producer cell lines in different media and culture modes (batch, fed-batch, semi-continuous) extracted from six publications [18–23]. We find that many fluxes in central carbon

metabolism can only be reliably estimated if non-growth associated cellular maintenance is considered which was so far not included in the GSMM.

Materials and methods

pFBA simulations

PFBA [24] was performed with the package COBRApy [25] using the solver Gurobi 9.1.0 [26] in python 3.7.9. The GSMM of CHO iCHO1766 [8] was used. Maximization of biomass production was used as the objective function using two biomass reactions available in the GSMM, `R_biomass_cho` and `R_biomass_cho_producing`. The main difference between these two reactions is that `R_biomass_cho` has lower protein content (56% compared to 70% in `R_biomass_cho_producing`), but higher lipid, DNA and RNA content. Uptake and secretion rates of extracellular metabolites and the recombinant product from 20 datasets (six publications) were used as constraints [18–23] (see [S1 Table](#) for an overview). In several cases, the uptake rates of tryptophan were not available. Assuming that it is the least abundant AA in the biomass [27], tryptophan uptake was constrained to the same value as the AA with the lowest uptake. All data were converted to $\text{mmol g}^{-1} \text{h}^{-1}$ using dry cell masses provided in the publications. If not available, the average mass of CHO (264 pg) was used [13]. In some cases, the experimental data for the exchange rates was not provided, so the fitted values from ^{13}C metabolic flux analysis (MFA) were used. If the data was provided only as plots, it was extracted using WebPlotDigitizer (<https://apps.automeris.io/wpd/>). Oxygen uptake was left unconstrained.

Mapping of ^{13}C models to iCHO1766

In order to compare predictions made by the GSMM of CHO to the results of ^{13}C MFA, it was necessary to map the metabolites and reactions from all models used for ^{13}C MFA (referred to as “ ^{13}C model” in the further text) to the GSMM of CHO iCHO1766 [8]. Metabolic flux data was extracted from six publications [18–23], see [S1 Table](#) for an overview.

For most models, it was impossible to make a one to one mapping. Thus, the following rules were applied.

- If one reaction in a ^{13}C model could be mapped to several reactions in iCHO1766, the fluxes from these reactions were summed up or subtracted, depending on the direction.
- In case of multiple equivalent reactions occurring in several compartments, their individual contributions predicted by PFBA were summed up and only the total was used for comparison. This approach disregards cellular compartments.
- In the ^{13}C models, several reactions are often lumped into one; therefore, the net flux of the corresponding reactions in the GSMM was calculated and compared to the flux of the lumped reaction.
- In case of producer cell lines, reactions for the synthesis of the recombinant protein were added comprising the AA composition provided in the publications and the energy demand for the polymerisation from [28] (2 GTP and 1.306 ATP per 1 mole of AAs are hydrolysed to 2 GDP, 1 AMP and 0.306 ADP).

Computational estimation of the maintenance energy

To estimate maintenance energy (mATP), PFBA was run for every individual dataset, where growth rate was maximized and mATP hydrolysis (reaction `R_DM_atp_`) was constrained to

a range of different values of mATP (0–40 mmol g⁻¹ h⁻¹ or until the simulation was no longer feasible). For each value of mATP, the agreement between experimental and predicted fluxes was evaluated and the value that led to the lowest median relative error was chosen as optimal. Reactions with the experimental fluxes less than 1% of the maximum flux ($|v_e^i/\max v_e^i| < 0.01$) were omitted from this analysis, because their absolute fluxes were very small (often close to zero) and consequently the relative errors were very high (even though the absolute differences in fluxes were very small). This often distorted the analysis and no clear minimum was observed. Additionally, the analysis was performed with all datasets at the same time—the mATP value was varied and the overall agreement between the predicted and the experimental fluxes for all datasets was evaluated. The calculated median errors were divided by the number of datasets for which a feasible solution was obtained (because the higher the mATP value, the lower the amount of datasets with a feasible pFBA solution).

Uptake objective function

PFBA simulations were done as in [29]. First, growth rate and productivity were fixed to the experimental values and the uptake of each essential AA was minimized one by one to get an estimate for the minimum uptake rate that sustains the experimental growth rate (nine AAs are essential in the iCHO1766 model). If the measured experimental uptake rate was lower than the minimum required uptake by the model, we fixed it to the computed uptake. Otherwise the experimental uptake rate was used. In a few cases, the uptake rates of tyrosine and cysteine had to be adjusted in the same way as the essential AAs, because the experimental uptake rates were insufficient to sustain growth and no solution was obtained (three datasets for tyrosine and three for cysteine).

In the next step, we constrained the nonessential uptake rates, secretion rates, growth rate and productivity to the experimental values (except for the nonessential uptake rate that was set as the objective, which was left unconstrained) and the essential uptake rates to the predicted or experimental values (see above). The flux distributions were obtained by performing pFBA with minimization of an uptake rate (glucose, glutamine, serine, tyrosine, arginine, aspartate or asparagine) as the objective.

Statistical analysis

Statistical analysis was carried out in R version 4.0.2. Linear correlations between experimental and predicted data were calculated with R function `lm`. In case of intracellular flux predictions, the inverses of the experimental confidence intervals were used as weights for the linear fitting. The relative error of the fluxes was calculated with Eq (1),

$$\frac{|v_p^i - v_e^i|}{|v_e^i|} \quad (1)$$

where v_p^i are the fluxes predicted by pFBA and v_e^i are the experimentally determined fluxes. Mean and median relative errors were calculated.

To check whether the addition of mATP constraint has a significant effect on the fits, mATP was added as a categorical predictor (value 0 or 1) and an interaction term was included in the model (experimental fluxes*mATP). If the term is significant (p-value < 0.05), we conclude that mATP has a significant effect on the slope. We also compared the models without or with mATP predictor with χ^2 analysis.

CHO cell cultivation

Suspension CHO-K1 cells (ECACC CCL-61) were grown in CD-CHO medium (Gibco, Thermo Fisher Scientific, MA, USA) supplemented with 0.2% (v/v) Anti-Clumping Agent (Gibco, Thermo Fisher Scientific, MA, USA) and 8 mM L-Glutamine (Sigma-Aldrich, MO, USA). Cells were cultivated in 125 mL non-baffled Erlenmeyer flasks at 37°C at 140 rpm with 25 mm throw, 7% CO₂ and 85% humidity and passaged every 2–4 days. Mycoplasma contamination was regularly checked with MycoAlert Mycoplasma Detection Kit (Lonza, Basel, Switzerland). The cell concentration and viability were determined with Vi-CELL XR (Beckman Coulter, CA, USA) calibrated with ViaCheck Concentration Control (Bangs Laboratories, Inc., IN, USA).

Continuous cultivation

Cells were cultivated in DASGIP Parallel Bioreactor System (Eppendorf, Hamburg, Germany) in DS0700ODSS vessels at 37°C and agitated with a marine impeller at 80 rpm. pH was monitored with EasyFerm Plus PHI K8 225 pH Electrode (Hamilton, NV, USA) and maintained at 7 ± 0.05 with CO₂ and 7.5% (w/w) NaHCO₃. pH was also checked with an external pH probe (Mettler Toledo) at least twice per week to correct potential pH drifts. Dissolved oxygen was measured with DO sensor VisiFerm (Hamilton, NV, USA) and maintained at 30% with a cascade (1. increase O₂ concentration in the incoming gas up to 50%, 2. increase both flow rate and O₂ concentration up to 75%, 3. increase flow rate up to 0.1 volume per volume per minute [vvm]). Cells were inoculated at a seeding density of 1.6×10^5 viable cells/mL at a working volume of 300 mL. At the end of the exponential phase, the culture was switched to the continuous mode and maintained at a constant volume of 270 mL. The flow-in pump was set to a constant rate and the amount of medium pumped into the bioreactors was monitored using Mettler Toledo balances MS6002TS (readability 0.01 g) to calculate an accurate flow rate into the bioreactors. The tube for flow-out was positioned at the height corresponding to 270 mL and the flow rate was set to a higher value than flow-in to prevent overflow. The feed medium was kept at room temperature and protected from light with aluminum foil. Due to the instability of glutamine, the medium was exchanged every 5–7 days. During this time frame, the glutamine degradation was shown to be negligible (see [S6 Fig](#)).

After changing the dilution rate, the cultures were left to equilibrate for at least five volume exchanges (except for one dilution rate (DR3, see [Table 1](#)) which was interrupted because of contamination). To verify whether the cultures reached steady state, linear fits were performed with viable cell density and Bioprofile data (glucose, lactate and ammonium concentrations) using R function `lm`. If the 95% confidence interval of the slope contained zero, the parameter was considered stable. For seven out of eleven dilution rates, all parameters were stable, including a dilution rate where only 2.5 volume exchanges were reached due to contamination (DR3). For three dilution rates $\frac{3}{4}$ parameters were stable, but the concentration changes of the unstable parameters were within the measurement error of the measurement device. Overall, all dilution rates were deemed stable enough and were used for further analysis (see [Table 1](#) for an overview).

Extracellular metabolites

The samples for supernatant analysis were taken at least at two time points per steady state. To separate cells from the medium, the cultures were centrifuged for 8 min at 200 g at room temperature and supernatants were stored at –80°C until further analysis or processed

Table 1. The dilution rates, calculated growth rates (Eq (3)), steady state concentrations of cells, metabolite exchange rates (Eq (4)) and carbon recovery.

ID	Dilution rate [h ⁻¹]	Growth rate [h ⁻¹]	Viable cells mL ⁻¹ 10 ⁻⁶	Glucose [mmol g ⁻¹ h ⁻¹]	Lactate [mmol g ⁻¹ h ⁻¹]	Ammonium [mmol g ⁻¹ h ⁻¹]	Carbon recovery
DR1	0.020	0.021	5.43	-0.42*	0.56	0.08	1.00
DR2	0.026	0.027	5.42	-0.44	0.53	0.09*	1.02
DR3	0.016	0.016	6.02	-0.32	0.31	0.06	0.71
DR4	0.027	0.028	6.06	-0.43	0.58	0.09	1.02
DR5	0.032	0.032	6.31	-0.48	0.57	0.11	1.02
DR6	0.033	0.033	5.83	-0.46	0.61	0.12	1.10
DR7	0.032	0.033	5.32	-0.46	0.70	0.12	1.12
DR8	0.023	0.023	11.37	-0.29	0.26	0.04	0.89
DR9	0.035	0.036	6.14	-0.54**	0.62**	0.09**	0.90
DR10	0.020	0.020	10.24	-0.28	0.27	0.04	0.89
DR11	0.024	0.024	9.77	-0.35*	0.34	0.04	0.85

A parameter was considered stable when the 95% confidence interval of the slope from the linear fit contained zero. Carbon recovery was calculated by summing up the total carbon uptake and subtracting the total carbon that is secreted or goes into biomass (based on growth rate and biomass composition from [13]).

* The slope was statistically significant, but the change in concentration of glucose and ammonium was within the measurement error of the Bioprofile analyzer.

** Confidence intervals could not be calculated because only two data points were available. The change in concentration was within the measurement error of the Bioprofile analyzer.

<https://doi.org/10.1371/journal.pcbi.1009022.t001>

immediately. Lactate, ammonium and glucose concentrations were measured at Bioprofile 100Plus (NOVA Biomedical, MA, USA). Lactate and ammonium measurements were corrected with 4-point calibration curves made in CD-CHO medium. As glucose was already contained in the CD-CHO medium, a calibration curve was not done. Instead, the average measured concentration of the standards was used for the calculation of the uptake rates in Eq (4).

For two dilution rates (DR1 and DR2), the AA concentrations were quantified by Biocrates with a commercial AbsoluteIDQ p180 kit. Briefly, AAs were derivatized with phenyl isothiocyanate in the presence of internal standards. The quantification was performed by liquid chromatography-mass spectrometry (LC-MS/MS) using a 4000 QTRAP (AB Sciex, Darmstadt, Germany) and a Xevo TQ-S micro (Waters, Vienna, Austria) instrument with an electrospray ionization source.

For the remaining dilution rates, AAs were analyzed using a high-performance liquid chromatography method. Briefly, samples were diluted, internal standards 3-(2-thienyl)-DL-alanine (Fluka) and sarcosine (Sigma) were added and subsequently filtered using a 0.2 µm filter unit (Sartorius). In an automated pre-column derivatization method, free primary AAs reacted with ortho-phthalaldehyde (OPA, Agilent) and proline and hydroxyproline with 9-fluorenyl-methyl chloroformate (FMOC, Fluka) and were then separated on a ZORBAX Eclipse Plus C18 column (Agilent) at 40 °C using a flow rate of 0.64 mL/min. After gradient elution with 10 mM K₂HPO₄:10mM K₂B₄O₇ (Merck) pH 8.2 as solvent A and acetonitrile:methanol:water (45:45:10, v:v:v) (Merck) as solvent B, AAs were excited at 230 nm and the fluorescence signal was detected at 450 nm for OPA derivates and 266 nm and 305 nm for FMOC derivates, respectively. Samples were quantified using an internal standard calibration.

The metabolite concentrations in the medium measured by both methods were compared to the patent for CD-CHO medium (Gibco, Thermo Fisher Scientific, MA, USA) to make sure the results are in the expected range and comparable between the two methods.

Calculation of growth rate and exchange rates

For all calculations, the average of all data points in each steady state was used. Dilution rate D was calculated with Eq (2),

$$D = F/V \quad (2)$$

where F is the flow rate into the bioreactors (calculated from the change of mass of the fresh culture medium over time) and $V = 270\text{mL}$ is the volume of the medium in the bioreactors. The growth rate μ at steady state was calculated with Eq (3),

$$\mu = DN_t/N_v \quad (3)$$

where N_v/N_t denotes fraction of viable cells. Steady state exchange rates q^i of extracellular metabolites were calculated with Eq (4),

$$q^i = (C_{\text{in}}^i - C_{\text{out}}^i)D/N_v \quad (4)$$

where C_{in}^i and C_{out}^i are concentrations of metabolites in the incoming medium and in the bioreactor, respectively. To calculate standard deviation (SD) for an exchange rate, the SDs were calculated for each variable from all available data points in steady state. Then, the SDs (σ) of the rate was calculated according to the mathematical rules of manipulation with standard deviations—Eq (5) if values were multiplied or divided (e.g. $C = AB$),

$$\sigma_c = \frac{1}{C} \sqrt{\left(\frac{\sigma_A}{A}\right)^2 + \left(\frac{\sigma_B}{B}\right)^2} \quad (5)$$

and Eq (6) if they were summed or subtracted (e.g. $C = A+B$)

$$\sigma_c = \sqrt{\sigma_A^2 + \sigma_B^2} \quad (6)$$

Determination of maintenance energy

The GSMM with cell line specific biomass composition from [13] was used (iCHO_K1par-8mMCD, BioModels ID: MODEL1907260016). The experimentally determined growth rate and the exchange rates of glucose, lactate, ammonium and AAs were used as constraints for flux balance analysis (FBA). The lower and upper bounds of the exchange reactions and the biomass reaction (`R_biomass_specific`) were fixed to the experimental values \pm SD. Due to high experimental noise, the uptake rates of some essential AAs were too low to sustain the experimental growth rate. Therefore the minimal uptake requirements were estimated as in [29] and, if necessary, the constraints were adjusted. This had no impact on the calculations of the ATP consumption as these AAs are solely used for biomass generation and not for ATP generation. In three cases, the lower bounds of secretion rates were relaxed (DR1—alanine secretion by 25%, DR5 glycine secretion by 40%, DR6 aspartate by 25%), otherwise the solutions would have been infeasible (the upper bounds were set to the experimental values).

After constraining the growth rate and extracellular exchange rates to the experimental values, pFBA was performed with maximization of ATP hydrolysis as the objective (reaction `R_DM_atp_`) for each dilution rate. Total ATP production was calculated by summing up fluxes of all reactions in the GSMM that produce nucleoside triphosphates (ATP, GTP, CTP, UTP, TTP, ITP, dATP, dGTP, dCTP, dUTP, dTTP, dITP; these compounds can be interconverted in the model) and plotted against growth rates. Linear fit was done in R (function `lm`). The intercept represents the estimated non-growth associated energy consumption (mATP) and 1/slope is biomass yield per mole of ATP corrected for mATP (Y_{ATP}^{max}).

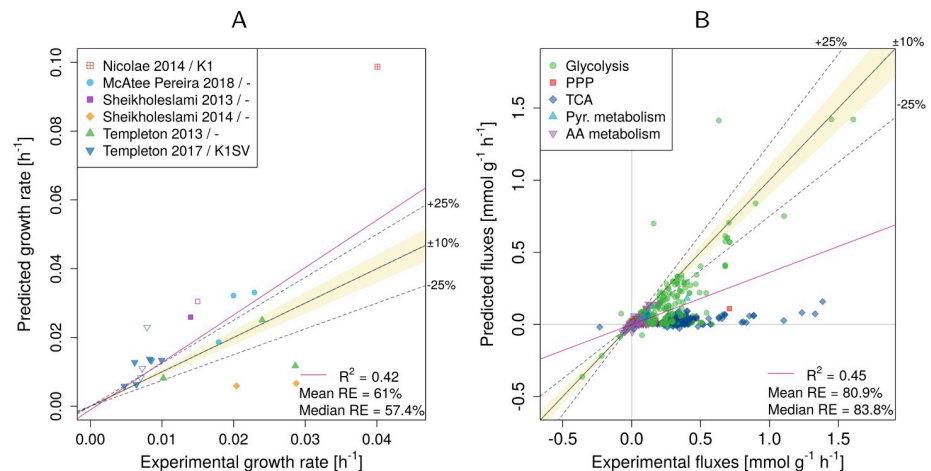


Fig 1. Experimental vs. predicted growth rates (A) and intracellular fluxes (B). Data is shown for biomass equation $R_{\text{biomass_cho}}$ as the objective function. RE—relative error. The legend in panel (A) indicates the publication and the used CHO cell line (if the information was available). Empty symbols indicate non-producers.

<https://doi.org/10.1371/journal.pcbi.1009022.g001>

Results

pFBA underestimates intracellular fluxes in *i*CHO1766

20 ^{13}C MFA datasets from producer and non-producer CHO cell lines across different media were collected from literature [18–23], see [S1 Table](#). Flux data were mapped onto the genome-scale metabolic model *i*CHO1766 [8] and compared to pFBA predictions based on biomass maximization (see [Methods](#)).

For 6 out of the 20 datasets growth could be predicted with an error of less than $\pm 25\%$ (for $R_{\text{biomass_cho}}$), see [Fig 1A](#). In three datasets growth was vastly underestimated, and overestimated in the remaining eleven. In one extreme case growth was overestimated by 190%. Overall the median relative error was close to 60%. pFBA performs even worse when compared to measured intracellular fluxes, hitting an overall median relative error of 83.8% ([Fig 1B](#)). On average, fluxes in glycolysis and AA are predicted better than fluxes in pentose phosphate pathway (PPP), pyruvate metabolism, and tricarboxylic acid cycle (TCA). More specifically, fluxes in PPP and TCA were vastly underestimated (median error 86.9% and 94.5%, see [Table 2](#)).

We checked whether flux predictions can be improved when experimental growth rates were used as additional constraints. Yet, no improvement was observed for those datasets that returned a feasible solution (median relative error 91.5% vs. 83.8% previously).

Table 2. R^2 and median relative error (Median RE) of the experimental and predicted fluxes with (+mATP) or without mATP (-mATP) as constraint. Data is shown for biomass equation $R_{\text{biomass_cho}}$.

Subsystem	-mATP		+mATP	
	R^2	Median RE (%)	R^2	Median RE (%)
Glycolysis	0.65	48.4	0.93	3.6
PPP	0.19	86.9	0.05	103
TCA	0.2	94.5	0.88	11
Pyr. metabolism	0.61	85.9	0.69	58.7
AA metabolism	0.72	63.6	0.74	36.2
All	0.45	83.8	0.93	24.6

<https://doi.org/10.1371/journal.pcbi.1009022.t002>

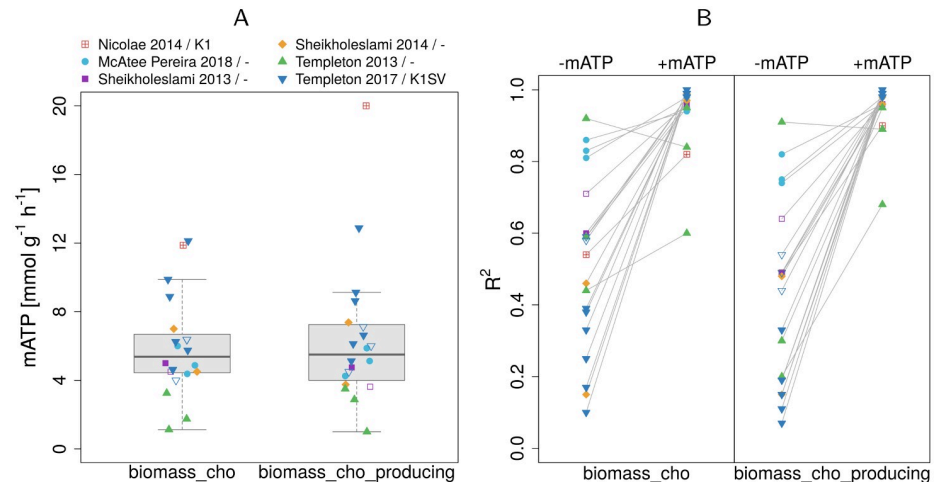


Fig 2. Estimated mATP values and their effect on flux prediction accuracy. (A) Computationally estimated mATP values for different datasets with two biomass equations. (B) R^2 values from linear fits of experimental and predicted intracellular fluxes without (-mATP) or with mATP (+mATP) as constraint. The legend indicates the publication and the used CHO cell line (if the information was available). Empty symbols indicate non-producers.

<https://doi.org/10.1371/journal.pcbi.1009022.g002>

Maintenance energy improves predicted glycolytic and TCA fluxes

The gross underestimation of intracellular fluxes, especially in glycolysis and TCA (supplementary S3 Fig), which are the major sources of ATP, points at an underestimation of the actual energy demand. In fact, current CHO models typically lack non-growth associated maintenance energy demands conventionally used in microbial models [30–32]. Thus, for each dataset we determined a CHO-specific, non-growth associated mATP by fixing the flux for the maintenance reaction (`R_DM_atp_c_`) such that the median relative error across all fluxes was minimal. S2 Fig illustrates data for the cell line SV-M3 [22]. For this cell line we find a maintenance demand of $5.75 \text{ mmol g}^{-1} \text{h}^{-1}$. Across all cell lines, mATP averages at 5.9 and $6.4 \text{ mmol g}^{-1} \text{h}^{-1}$ for `R_biomass_cho` and `R_biomass_cho_producing`, respectively (Fig 2A, S2 Table). Again the non-producing cell line CHO-K1 [20] sticks out with a more than three times larger maintenance energy demand compared to the average (across cell lines) for `R_biomass_cho_producing`.

Additionally we estimated a mean maintenance energy by fitting mATP across all datasets. Mean maintenance was very close to the average mATP determined for each individual dataset (5.75 for both biomass equations vs. 5.9 and $6.4 \text{ mmol g}^{-1} \text{h}^{-1}$ for `R_biomass_cho` and `R_biomass_cho_producing`, respectively).

Adding the estimated mATP value as a constraint strongly decreases the prediction errors in the intracellular fluxes for all but one dataset, see Fig 2B. More specifically, the overall median relative error decreased from 83.8% to 24.6% (Fig 3B) and from 92.5% to 16.6% for `R_biomass_cho` and `R_biomass_cho_producing`, respectively. Conversely, R^2 more than doubled from 0.45 and 0.41 to 0.93 and 0.95. The addition of mATP had a significant effect on the fit ($p\text{-value} < 2.2 \cdot 10^{-16}$), leading to a significant change of the slope from 0.36 to 0.98 for `R_biomass_cho` and from 0.27 to 1 for `R_biomass_cho_producing` (a value of 1 represents a perfect agreement between experimental and predicted fluxes).

Not only intracellular fluxes, but also growth rates were better predicted (Fig 3A). Now ten rather than previously only six out of 20 growth rates could be predicted with an error of less than $\pm 25\%$. Five were even predicted within an error band of $\pm 10\%$.

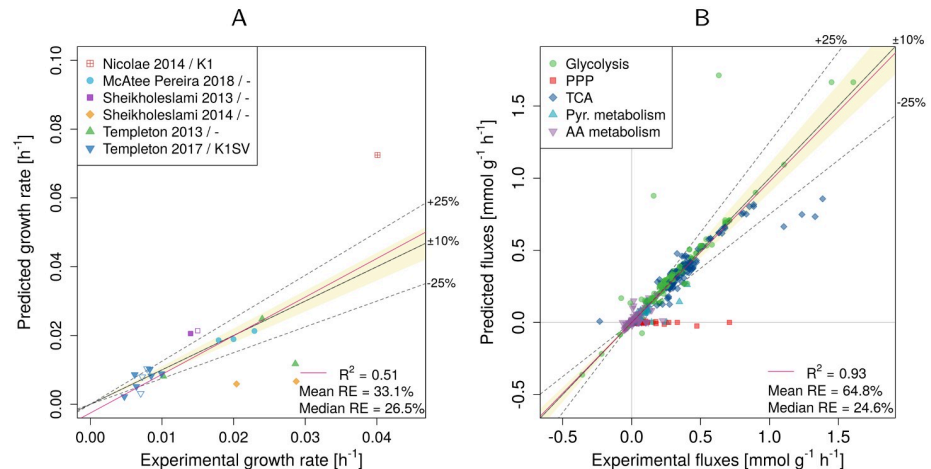


Fig 3. Experimental vs. predicted growth rates (A) and intracellular fluxes (B) after the addition of mATP as constraint. Results are shown for $R_{\text{biomass_cho}}$ as the objective function. RE—relative error. The legend in panel (A) indicates the publication and the used CHO cell line (if the information was available). Empty symbols indicate non-producers.

<https://doi.org/10.1371/journal.pcbi.1009022.g003>

While the predictions largely improved for TCA and glycolysis fluxes, PPP became inactive and the agreement with experimental data became worse (Table 2). However, the experimental data for PPP often have very big uncertainty—e.g. for Templeton 2013 [21], Templeton 2017 [22] and McAtee Pereira 2018 [23], which make 15 out of 20 datasets, the confidence intervals for the PPP reactions include zero.

Minimizing non-essential nutrient uptake performs similar to maximizing growth

Recently, minimizing uptake of non-essential nutrients (rather than maximizing growth) was suggested to be a more suitable modeling objective for CHO [29]. Thus, we repeated all previous simulations with uptake objective function (UOF), using the exchanges of glucose, glutamine, serine, tyrosine, asparagine, aspartate and arginine as objectives. Maintenance energy was estimated as before and similar mean mATP values were obtained (5.6–6.4 and 5.8–6.7 for the biomass equations $R_{\text{biomass_cho}}$ and $R_{\text{biomass_cho_producing}}$, respectively, S2 Table).

The prediction accuracy of the intracellular fluxes after the addition of the mATP constraint was comparable with biomass objective function (BOF) for all objective functions (see Fig 4B for an example with glucose UOF and S5 Fig for the remaining objectives).

The predictions of the minimum uptake rates were best for glucose with $R^2 = 0.92$ and a median relative error of 4.1% (Fig 4A), followed by glutamine ($R^2 = 0.75$, median error 50.4%) and asparagine ($R^2 = 0.12$, median error 24.2%). However, the uptake rates of the remaining AAs were not predicted well ($R^2 = 0.06$ or less; median errors within a range of 65.8–176%; S4 Fig).

Experimental determination of maintenance energy

To verify our computational estimate, we determined the maintenance energy experimentally in a CHO-K1 cell line. Continuous cultivation was run at eleven different dilution rates ranging from 0.016 to 0.035 h^{-1} (Table 1). Cell viability was above 95% for all steady states. The steady state viable cell densities were between 5.3 and 6.4×10^6 viable cells/mL for eight

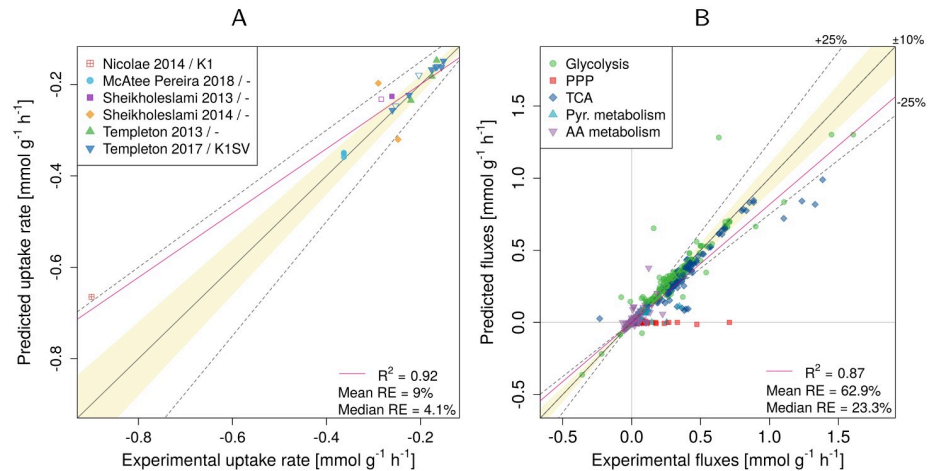


Fig 4. Experimental vs. predicted fluxes using minimization of glucose uptake rate as the objective function. (A) Experimental vs. predicted minimal glucosial uptake rate. (B) Experimental vs. predicted intracellular fluxes. Results are shown for $R_{biomass_cho}$ as the biomass reaction. RE—relative error. The legend in panel (A) indicates the publication and the used CHO cell line (if the information was available). Empty symbols indicate non-producers.

<https://doi.org/10.1371/journal.pcbi.1009022.g004>

dilution rates; for the remaining three they reached between $9.7\text{--}11.4 \times 10^6$ viable cells/mL (S7 Fig). For each dilution rate, extracellular exchange rates of glucose, AAs, lactate and ammonium were determined. Uptake of glucose, and glutamine as well as secretion of lactate and ammonium increased with increasing growth rate, see Fig 5. However, in case of waste product secretion rates, the three dilution rates that had higher steady state cell concentrations seem to separate from the remaining ones (indicated as magenta triangles in Fig 5).

Exchange rates of glucose, lactate, ammonium, all AA, and the growth rate were used as constraints for pFBA and the hydrolysis of ATP was maximized. The total ATP production was plotted against growth rate and a linear model was fitted (Fig 6). The intercept represents the non-growth associated ATP consumption—the estimated mATP and its standard error was determined to be $4.3 \pm 1.7 \text{ mmol g}^{-1} \text{ h}^{-1}$, which compares well with the average mATP of $5.9/6.4 \text{ mmol g}^{-1} \text{ h}^{-1}$ determined computationally above.

Because energy is partially generated via oxidative phosphorylation, the amount of produced ATP depends on the P/O ratio. In *i*CHO1766, P/O ratio for NADH is 2.5, which is a standard value [33]. To check how this value affects mATP estimation, we varied P/O ratio between 2–3 and obtained mATP values between $3.5\text{--}5 \text{ mmol g}^{-1} \text{ h}^{-1}$ (S8 Fig).

From the slope of Fig 6 we also calculated Y_{ATP}^{max} (growth yield per mole of ATP corrected for maintenance energy) and obtained value of $5.7 \pm 2.1 \text{ g mol}^{-1}$.

Discussion

An accurate determination of intracellular fluxes is key for understanding cellular metabolism and applying methods that predict engineering strategies. Intracellular fluxes can be experimentally determined with ¹³C metabolic flux analysis [34]. However, this method is very expensive due to the usage of labelled substrates and prone to experimental variability because of the need for rapid sampling and quenching of the metabolism. One of the cheaper and simpler methods for flux determination is pFBA [24], which first maximizes the biomass production (or other objective function) and subsequently minimizes the total sum of fluxes, based on the assumption that cells try to minimize the utilization of resources. This method was shown to be consistent with experimental data and it can be applied to GSMMs, which can

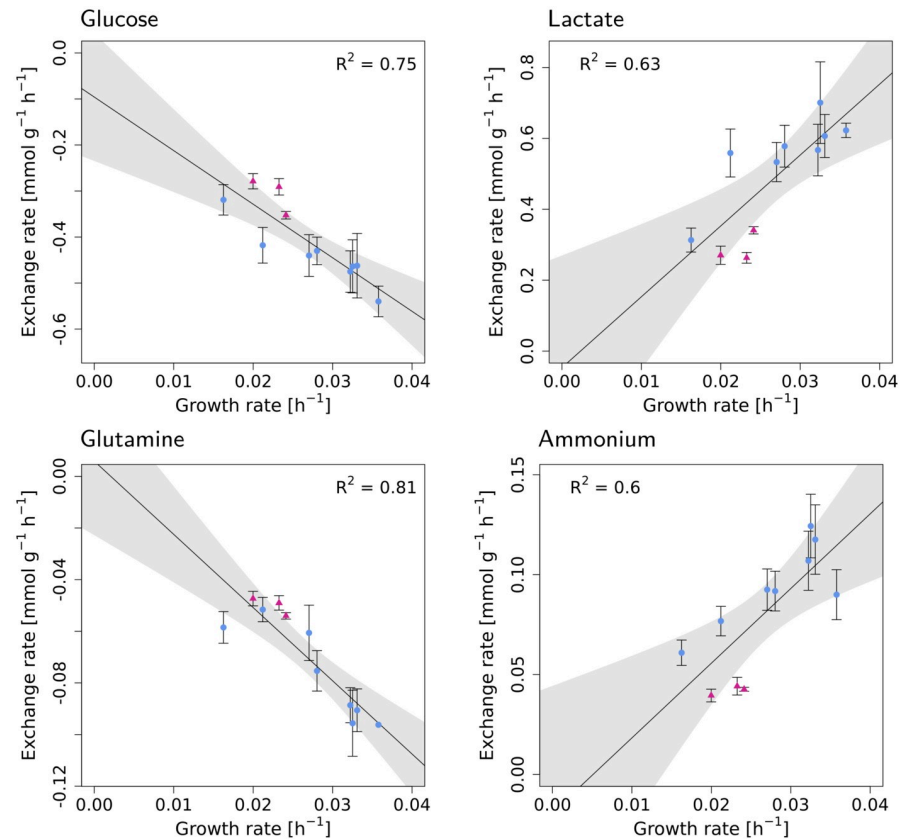


Fig 5. The experimental exchange rates of glucose (A), lactate (B), glutamine (C) and ammonium (D) increase with increasing growth rate. The shaded areas represent 95% confidence intervals. The triangle points in magenta color are the dilution rates that had unusually high cell concentration in steady state (see S7 Fig).

<https://doi.org/10.1371/journal.pcbi.1009022.g005>

provide a more complete picture about cell metabolism than the small models typically used for ¹³C MFA.

In this work, we evaluated the agreement between experimentally measured intracellular fluxes from 20 datasets [18–23] and pFBA predictions made with iCHO1766 genome-scale model. We observed that the fluxes of central carbon metabolism, especially TCA cycle, were underestimated in all datasets, which was explained by an insufficiently represented energy demand in the model. Although the iCHO1766 model takes into account energy demands for the synthesis of biomass and recombinant proteins, it currently lacks a value for non-growth associated maintenance energy—the energy needed for processes such as turnover and repair of macromolecules or maintenance of concentration gradients (e.g. Na⁺/K⁺ and Ca²⁺ ATPases) [35]. As no such value was available for CHO until now, we determined mATP computationally and experimentally.

The variability of the computationally estimated mATP across cell lines and conditions was quite high (relative SD 49% and 64% for R_biomass_cho and R_biomass_cho_producing, respectively). This might be the result of the experimental errors of the metabolite exchange rates. As seen in Fig 1A, the growth rate predictions had a high error, which we have shown previously to be sensitive to errors in the exchange rates [13, 14]. Another factor is the error of the ¹³C flux measurements which often had considerably big confidence intervals. The differences might also stem from differences in the cell lines, cultivation conditions or productivities. However, it was not possible to differentiate between biological effects on mATP

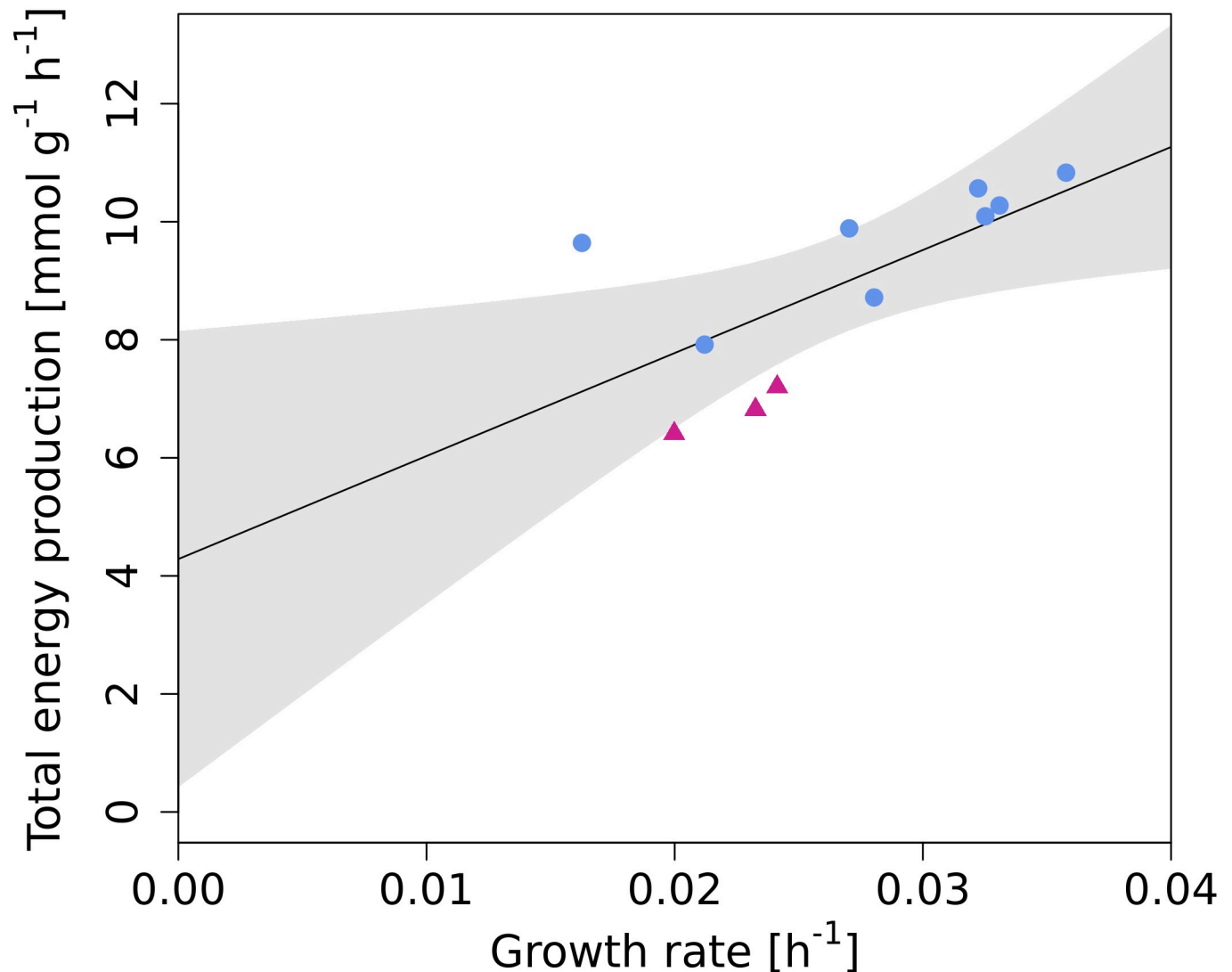


Fig 6. Total energy production at different growth rates (as indicated in Table 1). The black line is a linear fit and the intercept represents energy consumption at zero growth rate. The magenta triangles are dilution rates that had unusually high cell concentration in steady state (see S7 Fig). The shaded area represents 95% confidence interval.

<https://doi.org/10.1371/journal.pcbi.1009022.g006>

estimation (e.g. cell lines, conditions) from the effects caused by the differences in labelling and quantification (different labelled substrates, detection of intracellular vs. extracellular labelled metabolites) and modelling approaches (e.g. steady state vs. non-stationary modelling, presence of compartmentalisation). Nevertheless, the average mATP values were very similar when estimated with different biomass equations (Fig 2A) and lead to a major improvement in the predicted intracellular fluxes, especially in the TCA and glycolysis.

Fluxes of PPP got worse after the addition of a mATP constraint, which points at alternative NADPH sources connected to the TCA, e.g. NADP⁺-dependent malic enzyme (NADP-ME) or NADP⁺-dependent isocitrate dehydrogenase (NADP-ICDH). Indeed we found higher activity of NADP-ME and NADP-ICDH in some datasets, but not consistently in all. This points to a possible lack of actual NADPH demand in the model. Anabolic pathways that require NADPH, such as synthesis of lipids or nucleotides [36] are present in the model.

However, additional NADPH-consuming processes such as protein folding, degradation of misfolded proteins [37] or maintenance of cellular redox balance [38] are not represented in the model.

In our previous contribution [13] we observed that if glucose uptake and *all* amino acid exchange rates are accurately measured, growth rate predictions are accurate too as these rates essentially determine the energy metabolism even without considering mATP. Here we encountered several data sets where the inclusion of mATP improved growth predictions. However, since accuracy estimates on the exchange rates were sometimes missing in the original publications, we are unable to exclude simple measurement inaccuracies as the reason for this observation.

We also investigated the effect of alternative objective functions (nonessential uptake rates) suggested by Chen et al. [29]. The estimated mATP values and the predictions of intracellular fluxes were comparable to the predictions done with the “traditional” BOF for all tested objectives. However, the predictions of the minimum uptake rates worked much better for glucose uptake rate compared to the AA uptake rates. A possible explanation could be that the uptake rates of glucose are higher than the amino acid uptake rates, so the relative error is smaller and the predictions are less influenced by the noise in the input data.

The choice of the appropriate objective function might depend on the availability of experimental data. In case of using BOF, highly accurate uptake and secretion rates are needed in order to obtain accurate predictions, especially for essential AAs [13, 14]. If these are not available, using the UOF (glucose) might be a better choice than the use of BOF with imprecise AA uptake rates as constraints.

The experimentally determined mATP for CHO-K1 was comparable to the average computational estimate but much lower than the estimated mATP for CHO-K1 from Nicolae et al. [20] (Fig 2A). This discrepancy might have been caused by different experimental conditions, uncertainty in the exchange rates or due to conversion of the reported exchange rates from $\text{mmol L}_{\text{cell}}^{-1} \text{h}^{-1}$ to $\text{mmol g}^{-1} \text{h}^{-1}$ with a literature value for cell dry mass [13]. As an example, glucose uptake rate in Nicolae et al. was almost 1.7× higher than glucose uptake rate observed at the highest dilution rate in our continuous fermentation and 1.6× higher than the rate observed in batch cultivation of the same CHO-K1 cell line [13].

Furthermore, the uncertainty of the experimental estimate was quite high due to the technical difficulty of running continuous fermentation and the unstable nature of CHO cells. Long cultivations lead to cell clumping, which complicated cell counting. It is also known that CHO cells are unstable during long term cultivations [39, 40]. Furthermore, the physiological state of a culture during steady state might differ depending on how it was reached and different properties (e.g. cell and metabolite concentration) can be observed even if the same dilution rate and cultivation conditions are used [41–48]. Such multiplicity of steady states is likely a consequence of toxic waste product accumulation. Lower waste product secretion and higher cell densities indicate a metabolic switch to an energetically more efficient metabolism (higher activity of TCA and oxidative phosphorylation). This phenomenon could explain the different cell densities and exchange rates observed for three dilution rates (DR8, DR10 and DR11; S7 Fig and Fig 5). During the transitions between the different steady states, cells could have switched to a more oxidative metabolism with lower lactate secretion (or even consumption during the periods of transition). However, not enough data was available to investigate this phenomenon in more detail.

In literature there is only a small amount of data for mammalian maintenance energy and no data for CHO. Mouse cells require a maintenance energy of $1.7 \times 10^{-11} \text{ mmol cell}^{-1} \text{ d}^{-1}$ (65% of the total energy produced at the highest growth rate) [35], which corresponds to $1.1 \text{ mmol g}^{-1} \text{ h}^{-1}$ with a mouse cell dry mass (660 pg/cell) or 2.4–3.6 with a range of CHO dry

masses [13]. However, the analysis in [35] was quite simplified. Even though they cultivated the cells with a hydrolysate, they only considered glucose as the energy source and calculated the generated ATP from the secretion rates of lactate and CO₂. However, mammalian cells in culture will also use glutamine and other AAs as energy source [49].

Depending on the experimental/computational methods used, maintenance energy of cancer cells was estimated to be within 1.6 and 3.7 mmol g⁻¹ h⁻¹ [50, 51]. The values were converted from the original publications with CHO specific volume and dry mass values [13].

In other organisms, estimated/measured values widely vary and often depend on the cultivation conditions. In bacteria, the reported values range between 3.15–18.5 [30, 52–54], in yeast between 0.44–2.81 mmol g⁻¹ h⁻¹ [32, 55–57]. However, not only does mATP change across organisms and conditions but also during the batch as it is influenced by stress responses [31].

The estimated Y_{ATP}^{max} is close to previously reported values in yeast where it ranges from 8.6 g mol⁻¹ [58] up to 9.5 or 25.1 g mol⁻¹ depending on the carbon source [59]. Values for bacteria are also in a wide range between 10 to 31.9 g mol⁻¹, also depending on the carbon source [60]. To our knowledge, this information is not available for mammalian species up till now.

Finally, it is important to note that GSMMs have a large solution space. By computing a parsimonious flux distribution the space of possible solutions is reduced. That space can be further constrained by imposing mATP demand. However, some variability will remain (which may partially explain the variability in the mATP estimates). Hence, adding even more constraints could be beneficial for model performance. As an example, Lularevic et al. [61] reduced variability in flux variability analysis of *i*CHO1766 by adding carbon availability constraints. In another study, the predictions of intracellular fluxes were improved by adding constraints based on enzyme kinetic information [9]. This also led to a correct prediction of the overflow metabolism (the secretion of lactate). Together these studies, including the current one, show that adding more constraints to the models is necessary to fully capture cellular metabolism and leads to better predictions. Further developments and a combination of different approaches might lead to further improvement.

Conclusion

In this work we evaluated the prediction accuracy of CHO GSMM with pFBA. The intracellular fluxes were largely underestimated due to low energy demand and the missing non-growth associated maintenance energy was identified as the main reason for the bad flux predictions. The computationally estimated maintenance energy largely improved the predictions of central carbon metabolism and it was consistent with experimentally determined maintenance energy and with literature values for other mammalian cell lines. Adding this simple constraint to the model leads to a big improvement in the flux prediction accuracy and should not be neglected in constraint-based metabolic modeling of CHO.

Supporting information

S1 Table. Overview of the analysed ¹³C MFA datasets.

(XLSX)

S2 Table. Estimated mATP values with different objective functions.

(XLSX)

S1 Fig. Experimental vs. predicted growth rates (A) and intracellular fluxes (B). Data is shown for biomass equation `R_biomass_cho_producing` as the objective function. RE—relative error. The legend in panel (A) indicates the publication and the used CHO cell line

(if the information was available). Empty symbols indicate non-producers.
(TIF)

S2 Fig. An example of the computational estimation of mATP. mATP was gradually increased and the agreement between experimental and predicted fluxes was evaluated at each step. The mATP value that lead to the smallest median relative error of the fluxes was chosen as the optimal value. Data is shown for the dataset SV-M3 from Templeton 2017 [22] for biomass equation $R_{\text{biomass_cho}}$.
(TIF)

S3 Fig. Predictions of intracellular fluxes for the individual subsystems without (-mATP) or with mATP (+mATP) as constraint. Results are shown for $R_{\text{biomass_cho}}$ as the objective function. RE—relative error. Several outliers can be observed, which in most cases belong to a specific dataset. For example in glycolysis +mATP, the two most overestimated points belong to the “K1” dataset. In TCA +mATP, four underestimated points again belong to “K1” dataset, one to “early” dataset. In pyruvate metabolism +mATP, two underestimated points belong to “K1”, two to “early” datasets. In AA metabolism, the outliers belong to various datasets and sub-pathways.
(TIF)

S4 Fig. Predictions with different uptake rates as objective functions. Results are shown for $R_{\text{biomass_cho}}$ as the biomass reaction. RE—relative error. The legend indicates the publication and the used CHO cell line (if the information was available). Empty symbols indicate non-producers.
(TIF)

S5 Fig. Experimental vs. predicted intracellular fluxes using minimization of nonessential uptakes as objectives. Results are shown for $R_{\text{biomass_cho}}$ as the biomass reaction. RE—relative error.
(TIF)

S6 Fig. Glutamine degradation at room temperature. The concentration was measured with Bioprofile 100Plus (NOVA Biomedical, MA, USA). The degradation rate (slope of the linear fit) during this time frame is not significant (p-value = 0.402).
(TIF)

S7 Fig. Steady state viable cell density and viability at different growth rates.
(TIF)

S8 Fig. Estimated mATP (as in Fig 6) at different P/O ratios (NADH).
(TIF)

Author Contributions

Conceptualization: Michael Hanscho, Nicole Borth, Jürgen Zanghellini, David E. Ruckerbauer, Isabel Rocha.

Data curation: Diana Széliová.

Formal analysis: Diana Széliová, Jürgen Zanghellini.

Funding acquisition: Michael Hanscho, Nicole Borth, Jürgen Zanghellini, David E. Ruckerbauer.

Investigation: Diana Széliová, Jerneja Štor, Isabella Thiel, Michael Hanscho, Gabriele Lhota.

Methodology: Diana Széliová, Jerneja Štor, Marcus Weinguny, Michael Hanscho, Gabriele Lhota.

Project administration: Michael Hanscho, David E. Ruckerbauer.

Supervision: Michael Hanscho, Nicole Borth, Jürgen Zanghellini, David E. Ruckerbauer, Isabel Rocha.

Validation: Diana Széliová, Jerneja Štor, Gabriele Lhota, Jürgen Zanghellini.

Visualization: Diana Széliová.

Writing – original draft: Diana Széliová, Jürgen Zanghellini.

Writing – review & editing: Diana Széliová, Jerneja Štor, Marcus Weinguny, Michael Hanscho, Nicole Borth, Jürgen Zanghellini, David E. Ruckerbauer, Isabel Rocha.

References

1. Kuo CC, Chiang AW, Shamie I, Samoudi M, Gutierrez JM, Lewis NE. The emerging role of systems biology for engineering protein production in CHO cells. *Current Opinion in Biotechnology*. 2018; 51:64–69. <https://doi.org/10.1016/j.copbio.2017.11.015> PMID: 29223005
2. Walsh G. Biopharmaceutical benchmarks 2018. *Nat Biotechnol*. 2018; 36:1136–1145. <https://doi.org/10.1038/nbt.4305> PMID: 30520869
3. Lee JS, Kildegaard HF, Lewis NE, Lee GM. Mitigating Clonal Variation in Recombinant Mammalian Cell Lines. *Trends in biotechnology*. 2019;. <https://doi.org/10.1016/j.tibtech.2019.02.007> PMID: 30898338
4. Yusufi FNK, Lakshmanan M, Ho YS, Loo BLW, Ariyaratne P, Yang Y, et al. Mammalian systems biotechnology reveals global cellular adaptations in a recombinant CHO cell line. *Cell systems*. 2017; 4(5):530–542. <https://doi.org/10.1016/j.cels.2017.04.009> PMID: 28544881
5. Lai T, Yang Y, Ng SK. Advances in mammalian cell line development technologies for recombinant protein production. *Pharmaceuticals*. 2013; 6(5):579–603. <https://doi.org/10.3390/ph6050579> PMID: 24276168
6. O'Brien EJ, Monk JM, Palsson BO. Using genome-scale models to predict biological capabilities. *Cell*. 2015; 161(5):971–987. <https://doi.org/10.1016/j.cell.2015.05.019> PMID: 26000478
7. Gutierrez JM, Lewis NE. Optimizing eukaryotic cell hosts for protein production through systems biotechnology and genome-scale modeling. *Biotechnology journal*. 2015; 10(7):939–949. <https://doi.org/10.1002/biot.201400647> PMID: 26099571
8. Hefzi H, Ang KS, Hanscho M, Bordbar A, Ruckerbauer D, Lakshmanan M, et al. A Consensus Genome-scale Reconstruction of Chinese Hamster Ovary Cell Metabolism. *Cell Systems*. 2016; 3:434–443.e8. <https://doi.org/10.1016/j.cels.2016.10.020> PMID: 27883890
9. Yeo HC, Hong J, Lakshmanan M, Lee DY. Enzyme capacity-based genome scale modelling of CHO cells. *Metabolic Engineering*. 2020; 60:138–147. <https://doi.org/10.1016/j.ymben.2020.04.005> PMID: 32330653
10. Fouladiha H, Marashi SA, Li S, Li Z, Masson HO, Vaziri B, et al. Systematically gap-filling the genome-scale metabolic model of CHO cells. *Biotechnology Letters*. 2020. PMID: 33040240
11. Gutierrez JM, Feizi A, Li S, Kallehauge TB, Hefzi H, Grav LM, et al. Genome-scale reconstructions of the mammalian secretory pathway predict metabolic costs and limitations of protein secretion. *Nature Communications*. 2020; 11(1):1–10. <https://doi.org/10.1038/s41467-019-13867-y> PMID: 31896772
12. Kol S, Ley D, Wulff T, Decker M, Arnsdorf J, Schoffelen S, et al. Multiplex secretome engineering enhances recombinant protein production and purity. *Nature communications*. 2020; 11(1):1–10. <https://doi.org/10.1038/s41467-020-15866-w> PMID: 32313013
13. Széliová D, Ruckerbauer DE, Galleguillos SN, Petersen LB, Natter K, Hanscho M, et al. What CHO is made of: Variations in the biomass composition of Chinese hamster ovary cell lines. *Metabolic engineering*. 2020; 61:288–300. <https://doi.org/10.1016/j.ymben.2020.06.002> PMID: 32619503
14. Széliová D, Iurashev D, Ruckerbauer DE, Koellensperger G, Borth N, Melcher M, et al. Error propagation in constraint-based modeling of Chinese hamster ovary cells. *Biotechnology Journal*. 2021; 16(4):2000320. <https://doi.org/10.1002/biot.202000320> PMID: 33340257
15. Széliová D, Schoeny H, Knez Š Troyer C, Coman C, Rampler E, et al. Robust Analytical Methods for the Accurate Quantification of the Total Biomass Composition of Mammalian Cells. In: *Methods in*

- Molecular Biology. Springer US; 2020. p. 119–160. Available from: https://doi.org/10.1007/978-1-0716-0159-4_7.
16. Dikicioglu D, Kırdar B, Oliver SG. Biomass composition: the “elephant in the room” of metabolic modeling. *Metabolomics*. 2015; 11(6):1690–1701. <https://doi.org/10.1007/s11306-015-0819-2> PMID: 26491422
 17. Goudar CT, Biener R, Konstantinov KB, Piret JM. Error propagation from prime variables into specific rates and metabolic fluxes for mammalian cells in perfusion culture. *Biotechnology progress*. 2009; 25(4):986–998. <https://doi.org/10.1002/btpr.155> PMID: 19551875
 18. Sheikholeslami Z, Jolicoeur M, Henry O. Probing the metabolism of an inducible mammalian expression system using extracellular isotopomer analysis. *Journal of biotechnology*. 2013; 164(4):469–478. <https://doi.org/10.1016/j.jbiotec.2013.01.025> PMID: 23403402
 19. Sheikholeslami Z, Jolicoeur M, Henry O. Elucidating the effects of postinduction glutamine feeding on the growth and productivity of CHO cells. *Biotechnology Progress*. 2014; 30(3):535–546. <https://doi.org/10.1002/btpr.1907> PMID: 24692260
 20. Nicolae A, Wahrheit J, Bahnmann J, Zeng AP, Heinzle E. Non-stationary ¹³C metabolic flux analysis of Chinese hamster ovary cells in batch culture using extracellular labeling highlights metabolic reversibility and compartmentation. *BMC systems biology*. 2014; 8(1):50. <https://doi.org/10.1186/1752-0509-8-50> PMID: 24773761
 21. Templeton N, Dean J, Reddy P, Young JD. Peak antibody production is associated with increased oxidative metabolism in an industrially relevant fed-batch CHO cell culture. *Biotechnology and Bioengineering*. 2013; 110(7):2013–2024. <https://doi.org/10.1002/bit.24858> PMID: 23381838
 22. Templeton N, Smith KD, McAtee-Pereira AG, Dorai H, Betenbaugh MJ, Lang SE, et al. Application of ¹³C flux analysis to identify high-productivity CHO metabolic phenotypes. *Metabolic engineering*. 2017; 43:218–225. <https://doi.org/10.1016/j.ymben.2017.01.008> PMID: 28122259
 23. McAtee Pereira AG, Walther JL, Hollenbach M, Young JD. ¹³C Flux Analysis Reveals that Rebalancing Medium Amino Acid Composition can Reduce Ammonia Production while Preserving Central Carbon Metabolism of CHO Cell Cultures. *Biotechnology Journal*. 2018; 13(10):1700518. <https://doi.org/10.1002/biot.201700518>
 24. Lewis NE, Hixson KK, Conrad TM, Lerman JA, Charusanti P, Polpitiya AD, et al. Omic data from evolved *E. coli* are consistent with computed optimal growth from genome-scale models. *Molecular Systems Biology*. 2010; 6(1):390. <https://doi.org/10.1038/msb.2010.47> PMID: 20664636
 25. Ebrahim A, Lerman JA, Palsson BO, Hyduke DR. COBRApy: COstraints-Based Reconstruction and Analysis for Python. *BMC Systems Biology*. 2013; 7(1):74. <https://doi.org/10.1186/1752-0509-7-74> PMID: 23927696
 26. Gurobi Optimization L. Gurobi Optimizer Reference Manual; 2020. Available from: <http://www.gurobi.com>.
 27. Pan X, Dalm C, Wijffels RH, Martens DE. Metabolic characterization of a CHO cell size increase phase in fed-batch cultures. *Applied microbiology and biotechnology*. 2017; 101(22):8101–8113. <https://doi.org/10.1007/s00253-017-8531-y> PMID: 28951949
 28. Sheikh K, Förster J, Nielsen LK. Modeling Hybridoma Cell Metabolism Using a Generic Genome-Scale Metabolic Model of *Mus musculus*. *Biotechnology Progress*. 2008; 21(1):112–121. <https://doi.org/10.1021/bp0498138>
 29. Chen Y, McConnell BO, Dhara VG, Naik HM, Li CT, Antoniewicz MR, et al. An unconventional uptake rate objective function approach enhances applicability of genome-scale models for mammalian cells. *NPJ systems biology and applications*. 2019; 5(1):1–11. <https://doi.org/10.1038/s41540-019-0103-6> PMID: 31341637
 30. Varma A, Palsson BO. Stoichiometric flux balance models quantitatively predict growth and metabolic by-product secretion in wild-type *Escherichia coli* W3110. *Applied and environmental microbiology*. 1994; 60(10):3724–3731. <https://doi.org/10.1128/AEM.60.10.3724-3731.1994> PMID: 7986045
 31. Lahtee PJ, Kumar R, Hallström BM, Nielsen J. Adaptation to different types of stress converge on mitochondrial metabolism. *Molecular Biology of the Cell*. 2016; 27:2505–2514. <https://doi.org/10.1091/mbc.E16-03-0187> PMID: 27307591
 32. Tomàs-Gamisans M, Ferrer P, Albiol J. Fine-tuning the *P. pastoris* iMT1026 genome-scale metabolic model for improved prediction of growth on methanol or glycerol as sole carbon sources. *Microbial Biotechnology*. 2018; 11(1):224–237. <https://doi.org/10.1111/1751-7915.12871> PMID: 29160039
 33. Hinkle PC. P/O ratios of mitochondrial oxidative phosphorylation. *Biochimica et Biophysica Acta (BBA)-Bioenergetics*. 2005; 1706(1-2):1–11. <https://doi.org/10.1016/j.bbabi.2004.09.004> PMID: 15620362
 34. Wiechert W. ¹³C metabolic flux analysis. *Metabolic engineering*. 2001; 3(3):195–206. <https://doi.org/10.1006/mben.2001.0188> PMID: 11461141

35. Kilburn DG, Lilly MD, Webb FC. The Energetics of Mammalian Cell Growth. *Journal of Cell Science*. 1969; 4(3):645–654. <https://doi.org/10.1242/jcs.4.3.645> PMID: 5817088
36. Lunt SY, Vander Heiden MG. Aerobic glycolysis: meeting the metabolic requirements of cell proliferation. *Annual review of cell and developmental biology*. 2011; 27:441–464. <https://doi.org/10.1146/annurev-cellbio-092910-154237> PMID: 21985671
37. Elgaard L, Sevier CS, Bulleid NJ. How Are Proteins Reduced in the Endoplasmic Reticulum? *Trends in Biochemical Sciences*. 2018; 43(1):32–43. <https://doi.org/10.1016/j.tibs.2017.10.006> PMID: 29153511
38. Filosa S, Fico A, Pagliarunga F, Balestrieri M, Crooke A, Verde P, et al. Failure to increase glucose consumption through the pentose-phosphate pathway results in the death of glucose-6-phosphate dehydrogenase gene-deleted mouse embryonic stem cells subjected to oxidative stress. *Biochemical Journal*. 2003; 370(3):935–943. <https://doi.org/10.1042/BJ20021614> PMID: 12466018
39. Dahodwala H, Lee KH. The fickle CHO: a review of the causes, implications, and potential alleviation of the CHO cell line instability problem. *Current opinion in biotechnology*. 2019; 60:128–137. <https://doi.org/10.1016/j.copbio.2019.01.011> PMID: 30826670
40. Vcelar S, Jadhav V, Melcher M, Auer N, Hrdina A, Sagmeister R, et al. Karyotype variation of CHO host cell lines over time in culture characterized by chromosome counting and chromosome painting. *Biotechnology and bioengineering*. 2018; 115(1):165–173. <https://doi.org/10.1002/bit.26453> PMID: 28921524
41. Hayter PM, Curling EM, Baines AJ, Jenkins N, Salmon I, Strange PG, et al. Glucose-limited chemostat culture of chinese hamster ovary cells producing recombinant human interferon- γ . *Biotechnology and bioengineering*. 1992; 39(3):327–335. <https://doi.org/10.1002/bit.260390311> PMID: 18600949
42. Follstad BD, Balcarcel RR, Stephanopoulos G, Wang DI. Metabolic flux analysis of hybridoma continuous culture steady state multiplicity. *Biotechnology and Bioengineering*. 1999; 63(6):675–683. [https://doi.org/10.1002/\(SICI\)1097-0290\(19990620\)63:6%3C675::AID-BIT5%3E3.0.CO;2-R](https://doi.org/10.1002/(SICI)1097-0290(19990620)63:6%3C675::AID-BIT5%3E3.0.CO;2-R) PMID: 10397824
43. Europa AF, Gambhir A, Fu PC, Hu WS. Multiple steady states with distinct cellular metabolism in continuous culture of mammalian cells. *Biotechnology and bioengineering*. 2000; 67(1):25–34. [https://doi.org/10.1002/\(SICI\)1097-0290\(20000105\)67:1%3C25::AID-BIT4%3E3.0.CO;2-K](https://doi.org/10.1002/(SICI)1097-0290(20000105)67:1%3C25::AID-BIT4%3E3.0.CO;2-K) PMID: 10581433
44. Altamirano C, Illanes A, Casablanco A, Gamez X, Cairó JJ, Godia C. Analysis of CHO cells metabolic redistribution in a glutamate-based defined medium in continuous culture. *Biotechnology Progress*. 2001; 17(6):1032–1041. <https://doi.org/10.1021/bp0100981> PMID: 11735437
45. Namjoshi A, Kienle A, Ramkrishna D. Steady-state multiplicity in bioreactors: bifurcation analysis of cybernetic models. *Chemical Engineering Science*. 2003; 58(3-6):793–800. [https://doi.org/10.1016/S0009-2509\(02\)00609-7](https://doi.org/10.1016/S0009-2509(02)00609-7)
46. Gambhir A, Korke R, Lee J, Fu PC, Europa A, Hu WS. Analysis of cellular metabolism of hybridoma cells at distinct physiological states. *Journal of bioscience and bioengineering*. 2003; 95(4):317–327. [https://doi.org/10.1016/S1389-1723\(03\)80062-2](https://doi.org/10.1016/S1389-1723(03)80062-2) PMID: 16233414
47. Yongky A, Lee J, Le T, Mulukutla BC, Daoutidis P, Hu WS. Mechanism for multiplicity of steady states with distinct cell concentration in continuous culture of mammalian cells. *Biotechnology and bioengineering*. 2015; 112(7):1437–1445. <https://doi.org/10.1002/bit.25566> PMID: 25676211
48. Fernandez-de Cossio-Diaz J, Leon K, Mulet R. Characterizing steady states of genome-scale metabolic networks in continuous cell cultures. *PLoS computational biology*. 2017; 13(11):e1005835. <https://doi.org/10.1371/journal.pcbi.1005835> PMID: 29131817
49. Duarte TM, Carinhas N, Barreiro LC, Carrondo MJ, Alves PM, Teixeira AP. Metabolic responses of CHO cells to limitation of key amino acids. *Biotechnology and Bioengineering*. 2014; 111(10):2095–2106. <https://doi.org/10.1002/bit.25266> PMID: 24771076
50. Fernandez-de Cossio-Diaz J, Vazquez A. Limits of aerobic metabolism in cancer cells. *Scientific reports*. 2017; 7(1):1–8. <https://doi.org/10.1038/s41598-017-14071-y> PMID: 29044214
51. Fernandez-de Cossio-Diaz J, Vazquez A. A physical model of cell metabolism. *Scientific reports*. 2018; 8(1):1–13. <https://doi.org/10.1038/s41598-018-26724-7> PMID: 29844352
52. Hädicke O, Bettenbrock K, Klamt S. Enforced ATP futile cycling increases specific productivity and yield of anaerobic lactate production in *Escherichia coli*. *Biotechnology and bioengineering*. 2015; 112(10):2195–2199. <https://doi.org/10.1002/bit.25623> PMID: 25899755
53. Orth JD, Conrad TM, Na J, Lerman JA, Nam H, Feist AM, et al. A comprehensive genome-scale reconstruction of *Escherichia coli* metabolism—2011. *Molecular systems biology*. 2011; 7(1):535. <https://doi.org/10.1038/msb.2011.65> PMID: 21988831
54. Feist AM, Henry CS, Reed JL, Krummenacker M, Joyce AR, Karp PD, et al. A genome-scale metabolic reconstruction for *Escherichia coli* K-12 MG1655 that accounts for 1260 ORFs and thermodynamic information. *Molecular systems biology*. 2007; 3(1):121. <https://doi.org/10.1038/msb4100155> PMID: 17593909

55. Tomas-Gamisans M, Ferrer P, Albiol J. Integration and validation of the genome-scale metabolic models of *Pichia pastoris*: a comprehensive update of protein glycosylation pathways, lipid and energy metabolism. *PloS one*. 2016; 11(1):e0148031. <https://doi.org/10.1371/journal.pone.0148031> PMID: 26812499
56. Vos T, Hakkaart XD, de Hulster EA, van Maris AJ, Pronk JT, Daran-Lapujade P. Maintenance-energy requirements and robustness of *Saccharomyces cerevisiae* at aerobic near-zero specific growth rates. *Microbial cell factories*. 2016; 15(1):111. <https://doi.org/10.1186/s12934-016-0501-z> PMID: 27317316
57. Chung BK, Selvarasu S, Camattari A, Ryu J, Lee H, Ahn J, et al. Genome-scale metabolic reconstruction and in silico analysis of methylotrophic yeast *Pichia pastoris* for strain improvement. *Microbial cell factories*. 2010; 9(1):50. <https://doi.org/10.1186/1475-2859-9-50> PMID: 20594333
58. de Queiroz JH, Uribelarrea JL, Pareilleux A. Estimation of the energetic biomass yield and efficiency of oxidative phosphorylation in cell-recycle cultures of *Schizosaccharomyces pombe*. *Applied Microbiology and Biotechnology*. 1993; 39(4-5):609–614. <https://doi.org/10.1007/BF00205061>
59. Verduyn C. Physiology of yeasts in relation to biomass yields. *Antonie van Leeuwenhoek*. 1991; 60(3-4):325–353. <https://doi.org/10.1007/BF00430373> PMID: 1807201
60. Stouthamer AH. A theoretical study on the amount of ATP required for synthesis of microbial cell material. *Antonie van Leeuwenhoek*. 1973; 39(1):545–565. <https://doi.org/10.1007/BF02578899> PMID: 4148026
61. Lularevic M, Racher AJ, Jaques C, Kiparissides A. Improving the accuracy of flux balance analysis through the implementation of carbon availability constraints for intracellular reactions. *Biotechnology and bioengineering*. 2019; 116(9):2339–2352. <https://doi.org/10.1002/bit.27025> PMID: 31112296